Hybrid multiple-site mass closure and source apportionment of PM$_{2.5}$ and aerosol acidity at major cities in the Po Valley

Mauro Masiol [a,b,c,*], Stefania Squizzato [a,b,c], Gianni Formenton [d], Khan Md Badiuzzaman [c,e],
Philip K. Hopke [b,f], Athanasios Nenes [a,g], Spyros N. Pandis [a,h,i], Laura Tositti [j], Francesca Benetello [c],
Flavia Visin [c], Bruno Pavoni [c]

[a] Institute of Chemical Engineering Sciences, Foundation for Research and Technology – Hellas (FORTH), GR-26504 Patras, Greece
[b] Department of Public Health Sciences, University of Rochester Medical Center, Rochester, NY 14642, United States
[c] Dipartimento di Scienze Ambientali, Informatica e Statistica, Università Ca' Foscari Venezia, IT-30170 Mestre-Venezia, Italy
[d] Dipartimento Regionale Laboratori, Agenzia Regionale per la Prevenzione e Protezione Ambientale del Veneto (ARPAV), IT-30174 Mestre-Venezia, Italy
[e] Department of Environmental Science, Bangladesh Agricultural University, Mymensingh 2202, Bangladesh
[f] Center for Air Resources Engineering and Science, Clarkson University, Potsdam, NY 13699-5708, United States
[g] Laboratory of Atmospheric Processes and Their Impacts, School of Architecture, Civil and Environmental Engineering, École Polytechnique Fédérale de Lausanne, Lausanne, CH-1015, Switzerland
[h] Department of Chemical Engineering, University of Patras, Patras, Greece
[i] Department of Chemical Engineering, Carnegie Mellon University, Pittsburgh, PA 15213, USA
[j] Dipartimento di Chimica "G. Ciamician", Alma Mater Studiorum Università di Bologna, IT-40126 Bologna, Italy

HIGHLIGHTS

- The addition of aerosol water content returns reasonable mass closures.
- Six common PM$_{2.5}$ sources are present over 5 cities in the lower end of Po Valley.
- Aerosol is acidic/moderately acidic throughout the year with lower pH in summer.
- Sulfate and fossil fuel lower pH; nitrate and biomass burning increase pH.
- Secondary sources and pH increase when air masses pass Central/Eastern Europe.

GRAPHICAL ABSTRACT
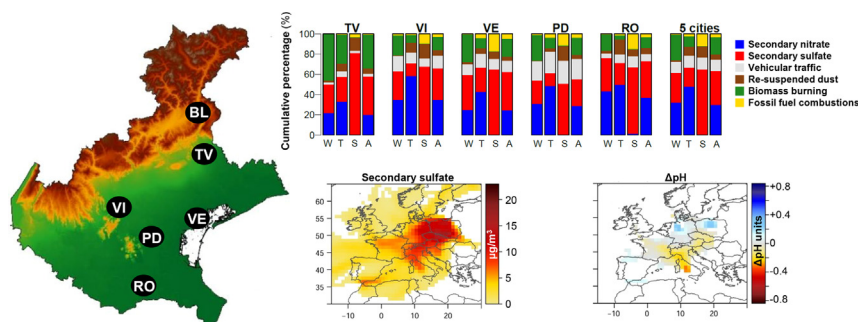
ARTICLE INFO

ABSTRACT

This study investigates the major chemical components, particle-bound water content, acidity (pH), and major potential sources of PM$_{2.5}$ in major cities (Belluno, Conegliano, Vicenza, Mestre, Padua, and Rovigo) in the eastern end of the Po Valley. The measured PM$_{2.5}$ mass was reconstructed using a multiple-site hybrid chemical mass closure approach that also accounts for aerosol inorganic water content (AWC) estimated by the ISORROPIA-II model. Annually, organic matter accounted for 31–45% of the PM$_{2.5}$ at all sites, followed by nitrate (10–19%), crustal material (10–14%), sulfate (8–10%), ammonium (5–9%), elemental carbon (4–7%), other inorganic ions (3–4%), and trace elements (0.2–0.3%). Water represented 7–10% of measured PM$_{2.5}$. The ambient aerosol pH varied from 1.5 to 4.5 with lower values in summer (average in all sites 2.2 ± 0.3) and higher in winter (3.9 ± 0.3). Six major PM$_{2.5}$ sources were quantitatively identified with multiple-site positive matrix factorization: secondary sulfate (34% of PM$_{2.5}$), secondary nitrate (30%), biomass burning (17%), traffic (11%), re-suspended dust (5%), and fossil fuel combustion

* Corresponding author at: Dipartimento di Scienze Ambientali, Informatica e Statistica, Università Ca' Foscari Venezia, c/o INCA-VEGAPARK, via delle Industrie, 21/8, IT-30170 Marghera (VE), Italy.
E-mail address: mauro.masiol@unive.it (M. Masiol).

Water content

(3%). Biomass burning accounted for ~90% of total PAHs. Inorganic aerosol acidity was driven primarily by secondary sulfate, fossil fuel combustion (decreasing pH), secondary nitrate, and biomass burning (increasing pH). Secondary nitrate was the primary driver of the inorganic AWC variability. A concentration-weighted trajectory (multiple-site) analysis was used to identify potential source areas for the various factors and modeled aerosol acidity. Eastern and Central Europe were the main source areas of secondary species. Less acidic aerosol was associated with air masses originating from Northern Europe owing to the elevated presence of the nitrate factor. More acidic particles were observed for air masses traversing the Po Valley and the Mediterranean, possibly due to the higher contributions of fossil fuel combustion factor and the loss of nitric acid due to its interaction with coarse sea-salt particles.

1. Introduction

During the past several decades, air quality has improved across Europe (Colette et al., 2011; Giannouli et al., 2011; Colette et al., 2016). The downward trends of air pollution are due to increasingly stringent policies and abatement measures mandated by the European Union and the implementation of increasingly effective emission control technologies in industry, road, and off-road transport (Turnock et al., 2016; Crippa et al., 2016). However, the European standards for air quality remain exceeded at hotspots like the Po Valley in Northern Italy (EEA, 2014, 2016, 2018).

The Po Valley can be considered an extended megacity (WMO/IGAC, 2012), where anthropogenic polluting activities are densely spread over a 46×10^3 km^2-wide floodplain/hilly territory hosting around 16 million inhabitants. Mountains surround the valley to the north and west (Alps), and south (Apennines), while the east side is open to the Adriatic Sea. This topography favors air stagnation events and is accompanied by frequent wintertime thermal inversions and widespread fog events leading to the buildup of particulate matter (PM) pollution (Carbone et al., 2010; Pernigotti et al., 2012; Larsen et al., 2012; Squizzato et al., 2013; Pecorari et al., 2013; Perrino et al., 2014).

The Veneto region (~18.4×10^3 km^2) lies at the eastern end of the Po Valley, i.e. the side open to the sea over a ~95 km-long coastline (Fig. S1a). The population resides in several major cities and in a large number of smaller towns and villages scattered across the floodplain (Fig. S1b,c). The northwestern territories are alpine environments with a low population density mostly concentrated along narrow valleys. A hilly belt hosting semirural environments, farming (vineyards and orchards) and small/medium sized villages is located between the floodplain and the Alps.

The Veneto region is affected by multiple emission sources; urban and industrial areas are mixed with intensive farming and semi-rural areas (Fig. S1c). Traffic emissions can be found throughout the region (Fig. S1d) due to a dense local road network and the presence of international roads and transport hubs. Off-road emissions from railways are low because the network is electrified, although some diesel-powered trains still operate. Shipping emissions due to cruise ships and maritime freight transport are concentrated in the Lagoon of Venice. Natural gas is the main fuel used for domestic/commercial heating, while diesel/oil is still used in the more rural areas. Residential wood combustion is frequent in the hilly and mountainous areas. Wood combustion using small traditional stoves, pellet stoves, closed or open fireplaces is also becoming popular in the major cities of the valley as a cheaper alternative to natural gas. Large industries are located close to the main cities (Venice-Mestre, Padua, and Vicenza), while medium and small factories are scattered across the region, each with different emission characteristics (Supplementary material Section S1).

The European PM$_{2.5}$ limit value of 25 μg m^{-3} (annual average) was frequently exceeded at various sites between 2009 and 2014 (Masiol et al., 2017). Almost all prior studies of PM$_x$ chemical composition and sources have been performed in the region's capital metropolitan area, Venice or Mestre (Stortini et al., 2009; Masiol et al., 2012; 2014a; Squizzato et al., 2014) resulting in a lack of information for the other major cities. It is still unclear if: (i) the PM$_{2.5}$ concentration is driven by local sources or transport of pollution from other areas; and (ii) the same sources are present across the urban areas of the region or if each city has different local sources. There is clearly a need to investigate the PM$_{2.5}$ composition and sources concurrently at multiple sites across the region.

Aerosol acidity plays a key role in the physical and chemical properties of PM as well as controlling the redox state and solubility of PM-bound elements (Nenes et al., 2011; Shi et al., 2012; Oakes et al., 2012; Li et al., 2017; Fang et al., 2017; Ito et al., 2019). Transition metals (e.g., Fe, Cu, Mn) are usually emitted in insoluble form, but their solubilization can be enhanced in acidic particles. In soluble form, those elements become more bioactive, affecting both the productivity of ecosystems upon deposition and the oxidative potential of inhaled PM and associated adverse health effects through the generation of reactive oxygen species in vivo (Hopke, 2015a; Lakey et al., 2016; Fang et al., 2017). Aerosol acidity in Italy has received little attention so far (Squizzato et al., 2013).

This study presents PM$_{2.5}$ chemical speciation data from in 6 major cities in the Veneto to:

- Estimate the PM$_{2.5}$ aerosol water content (AWC) and *in-situ* acidity (pH);
- Reconstruct the measured PM$_{2.5}$ mass from the analyzed species accounting for AWC at the conditions of the gravimetric determination;
- Identify and quantify the major PM$_{2.5}$ sources;
- Estimate the impacts of the various sources on AWC and aerosol acidity; and
- Identify the location of the major sources and the potential effect of regional/transboundary transport on aerosol acidity.

2. Measurements and data analysis

2.1. Site characteristics

PM$_{2.5}$ samples were collected at 6 sites managed by the local environmental protection agency (Agenzia Regionale per la Prevenzione e Protezione Ambientale del Veneto, ARPAV) (Fig. S1). Site characteristics are listed in Table S1 and are discussed in Section S1; the average population density and percent land cover within a 5 km radius from each site are shown in Fig. S2. The 2013 emission inventories for some major sectors are summarized in Table S2.

Belluno (BL, 36,600 inhabitants) is in an Alpine valley (altitude above sea level 390 m) surrounded by mountains (height 700 to 2500 m) and dominated by cultivated crops and forests. Conegliano (TV, 35,700 inhabitants) is a medium-sized city in the hilly

belt. Land cover is dominated by agricultural areas (mostly vine-yards and orchards), but there are also small and medium-sized factories (stainless steel process, appliances, electrical equipment). Vicenza (VI, 115,900 inhabitants) is a large city in the foothills hosting small to medium-sized mechanical, textile, tanning and jewelry manufactures. The site is in a dense urban area. Venice-Mestre (VE, 271,000 inhabitants) is located on the coast of the Lagoon of Venice. The site was placed in a public park surrounded by a densely populated area located north of a large industrial zone (chemical, steel, oil-refinery, incineration, thermoelectric power plants and others). A 13 years-long data analysis at this site (Masiol et al., 2014b) showed that air quality was affected primar-ily by residential/building heating, traffic, and industrial emissions. Padua (PD, 214,200 inhabitants) is characterized by the highest urban coverage and population density (Fig. S2). PD is affected by heavy traffic from local roads and a logistics hub for trucks, and many medium-sized factories. Rovigo (RO, 52,800 inhabitants) is located in an agricultural environment with several small-medium factories (food processing, metalworking, carpentry, tex-tile, and construction).

2.2. Methods

A one year-long sampling campaign (April 2012 to March 2013) was performed at each site according to the EN14907:2005 stan-dard using quartz fiber filters (Whatman QMA). Every day sam-pling was continuous for 24-h starting at midnight. PM mass was measured gravimetrically (48 h conditioning at 20 ± 1 °C and 50 ± 5% RH). Six periods representative of the different seasons were selected for the analysis: winter (December and February), summer (June and August), and transition (April and October).

For each sample, a ~2 cm^2 punch was extracted in ultrapure water (specific resistivity 18 MΩ cm) and analyzed for NO_3^-, SO_4^{2-}, F^-, Cl^-, Na^+, NH_4^+, K^+, Mg^{2+}, and Ca^{2+} by ion-exchange chromatogra-phy (Masiol et al., 2015). EC/OC was analyzed in 1 cm^2 punches using a carbon aerosol analyzer (Sunset Lab, USA) adopting the NIOSH-5040 protocol (Birch and Cary, 1996). A ~2 cm^2 punch was extracted in acetonitrile and analyzed for 8 PAHs (benz(a)an-thracene (BaA), chrysene (Chry), benzo(b)fluoranthene (BbF), benzo(k)fluoranthene (BkF), benzo(a)pyrene BaP, indeno(1,2,3-c,d)pyrene (IP), dibenzo(a,h)anthracene (DBahA) and benzo(g,h,i) perylene (BghiP)) by a HPLC interfaced with a multi-wavelength fluorescence detector (Masiol et al., 2013). The remaining portion of each filter was subjected to acid digestion (HNO_3-HF-H_2O_2) in a microwave oven and was analyzed for 10 elements (Mg, Al, S, K, Ca, Ti, Mn, Fe, Zn, Ba) in inductively coupled plasma optical emission spectroscopy and 8 elements (V, Co, Ni, Cu, As, Cd, Sb, Pb) in inductively coupled plasma mass spectrometry. Details can be found in Squizzato et al. (2014) and Benetello et al. (2018).

Statistical analyses were performed using R 3.5.1 (R Core Team, 2018) and a number of packages, including "MASS" (Venables and Ripley, 2002), "scales" (Wickham, 2018), "plyr" (Wickham, 2011), "zoo" (Zeileis and Grothendieck, 2005), "lubridate" (Grolemund and Wickham, 2011), "reshape" (Wickham, 2007), "rcompanion" (Mangiafico, 2019), "dunn.test" (Dinno, 2017), "openair" (Carslaw and Ropkins, 2012), "car" (Fox and Weisberg, 2011), "NISTunits" (Gama, 2016), "boot" (Canty and Ripley, 2017), "DAAG" (Maindonald and Braun, 2019), and "Hmisc" (Harrell et al., 2018).

2.3. QA/QC

The quality of the analytical procedures was checked by blank controls, by evaluating detection limits, recoveries, accuracy, and repeatability. Calibration curves were generated before and during each batch of analysis with analytic-grade standards. The accuracy of quantitative analyses was assessed by analyzing certified liquid standards (TraceCERT, Fluka) for water soluble ions, sucrose (ana-lytical grade) for EC/OC, certified reference material ERM CZ100 (JRC, Belgium) for PAHs, and standard reference materials SRM1648 (NIST, USA) for the various elements. The recoveries of ions and elements were in the 80–110% range; PAHs recovery effi-ciencies varied from 75% to 125%. The relative standard deviation (10 replications) of ions, elements and PAHs was < 5%.

2.4. Ancillary variables

Insoluble K and Ca were estimated by subtracting the ionic con-centration from the corresponding bulk concentration. The partic-ulate anion equivalent (AEq, expressed as $\mu eq\ m^{-3}$; Kerminen et al., 2001) was calculated as the sum of equivalents of nitrate, sulfate and chloride.

Weather data including air temperature (°C), relative humidity (RH), wind speed/direction, and solar radiation (W m^{-2}) were recorded at weather stations as close as possible to the sites (Fig. S3). Daily average values were calculated when more than 75% of the hourly data were available.

2.5. Aerosol water content and acidity

The AWC and pH can be estimated combining an aerosol ther-modynamic model and the measured particle composition with air temperature and humidity assuming that the aerosol system is in equilibrium. In this study, ISORROPIA-II (Nenes et al., 1998; Fountoukis and Nenes, 2007) was used in the "*forward*" mode assuming that the particles are in the "*metastable*" phase state to predict both the hydronium ion concentration per volume of air (H_{air}^+; μg m^{-3}) and the concentration of particle liquid water (AWC; μg m^{-3}). pH is then estimated as:

$$pH \cong -\log_{10} \frac{1000 \gamma_{H^+} H_{air}^+}{AWC} \qquad (1)$$

where γ_{H^+} is the hydronium ion activity coefficient (assumed to be equal to 1). In this study, we used the following assumptions: (i) we neglected any contribution of the organics (thus this study assesses the "inorganic" pH and AWC not accounting for the organic PM$_{2.5}$ fraction), (ii) we neglected possible differences in composition with particle size in the PM$_{2.5}$ range, and (iii) we used the daily-averaged air temperature and RH to match the 24-h samples. The calculation of the aerosol pH using only the particulate composition, when no measurements of gas-phase NH$_3$, HNO$_3$, and HCl are available, can be quite sensitive to small experimental errors. For this reason, we ran the model twice, to bind the likely pH range: (i) a "base" simulation with only the particulate composition and no gaseous species, and (ii) a "sensitivity" test using the highest concentrations of ammonia (the species that mostly affects the aerosol pH) reported for some semirural and urban areas of Veneto (ARPAV, 2016). ISORROPIA-II has been used like this in several previous studies (Guo et al., 2015, 2016; Weber et al., 2016; Bougiatioti et al., 2016; Fang et al., 2017; Ding et al., 2019).

Since pH depends on air temperature and RH, it often shows a strong seasonal dependence. To remove this dependence, ΔpH (Shi et al., 2017) is calculated as the difference between pH and the acidity estimated using the actual meteorology (temperature and RH) and the annual average composition (pH*):

$$\Delta pH_{i,t} = pH(C_{i,t}, T_{i,t}, RH_{i,t}) - pH^*(\bar{C}_i, T_{i,t}, RH_{i,t}) \qquad (2)$$

where $C_{i,t}$ is the ion + gas composition at site i and sample t, $T_{i,t}$, $RH_{i,t}$ are the air temperature and RH at site i for sample t, and $\bar{C}_i$ is the average ion + gas composition over the study period (calculated as in the equation (1)). Analogous to ΔpH, ΔAWC was calculated to remove the seasonal dependence by subtracting AWC* that is

the water estimated using the average chemical composition and the temperature, RH corresponding to the specific sample:

$$\Delta AWC_{i,t} = AWC(C_{i,t}, T_{i,t}, RH_{i,t}) - AWC^*\left(\bar{C}_i, T_{i,t}, RH_{i,t}\right) \qquad (3)$$

2.6. Mass closure

Mass closure aims to compare the measured $PM_{2.5}$ mass concentration with the sum of the concentrations of the measured components with assumptions to account for not measured elements, mostly hydrogen and oxygen in both organic and inorganic compounds as well as the AWC (Harrison et al., 2003; Yin and Harrison, 2008; Chow et al., 2015). In this study, hybrid-mass closure (hyb-MC), also accounting for AWC, was calculated for each site and for all the sites together (multiple-site hyp-MC, MS-hyb-MC). The reconstructed $PM_{2.5}$ mass (RM_{hyb}) was estimated by summing the organic matter (OM), crustal or geological material (CRU), nitrate, sulfate, ammonium, other ions (OI), trace elements (TRACE), and also including AWC. OM was calculated over the whole year by multiplying OC by 1.6 (Hand and Malm, 2007; Vecchi et al., 2008; Perrone et al., 2012; Perrino et al., 2014; Squizzato et al., 2016). Although this coefficient likely varies by season, there was no clear basis for assigning alternative values. CRU was calculated by converting the crustal-like elements (Si, Al, Fe, Ti, K, and Ca) to the respective geochemical oxides (Table S3). The AWC at the conditions of the gravimetric analysis, AWC_{std}, was computed by running ISORROPIA-II ("*forward*", "*metastable*") with a constant RH (50%) and temperature (20 °C). AWC_{std} was also estimated for the sensitivity test assuming a high concentration of gas-phase NH_3.

2.7. PMF

In this study, US EPA PMF version 5 was used (Paatero and Tapper, 1994; Paatero, 1997; Hopke, 2015b; 2016). Uncertainties for chemical species were assessed according to Polissar et al. (1998): for concentrations above the detection limits (DL), uncertainties were determined by adding DL/3 to the errors of the corresponding analytical procedures. Concentrations below the DL were set as DL/2, with an uncertainty of 5/6 of the corresponding DL plus the addition of DL/3. Variables were preliminarily screened for their information content (Paatero and Hopke, 2003): species having signal-to-noise ratio less than 0.5 were removed from the analysis, those with 0.5 < S/N < 1 were marked as "weak" (tripling their uncertainty). Uncertainty for the total $PM_{2.5}$ was set to 300% of the concentration to prevent it from driving the model (Kim et al., 2003). Extra-modeling uncertainty was added to encompass errors not considered in the uncertainty assessment; solution diagnostics were tested with increasing extra uncertainty from 0% to 20%.

The optimal PMF solution was identified based on (i) the minimization of differences between measured and expected (theoretical) Q-values; (ii) the stability of solutions over 200 runs; (iii) the minimization of the number of absolute scaled residuals exceeding ±3; (iv) accepting source profiles with physical meaning with respect to the known sources impacting the study area; (v) the stability of profiles over multiple runs; (vi) the uncertainties of profiles within an acceptable range as calculated by bootstrap (BS, n = 300) displacement (DISP), and combined BS-DISP methods (Paatero et al., 2014); (vii) the absence of unmapped BS factors, and (viii) the minimization of swaps in BS (<8%) (Reff et al., 2007; Belis et al., 2014; Brown et al., 2015; Hopke, 2016). Rotational ambiguities were investigated by checking the G-space (Paatero et al., 2005), DISP and BS-DISP results (Brown et al., 2015). The ranges (min–max) of the adjustment in factor profile values obtained in DISP with the constraint that the difference

(dQ = base-modified) is no greater than the dQ_{max} = 4 were used to assess the uncertainty boundaries associated to the final PMF profiles.

2.8. Multiple-site concentration weighted trajectory

Back-trajectories (-120 h, model vertical velocity, starting height 500 m above ground level) were computed using the NOAA/ARL HYSPLIT4 model (Rolph et al., 2017; Stein et al., 2015). Meteorological data were retrieved from the NCEP/NCAR Reanalysis Data (Kalnay et al., 1996). The concentration weighted trajectory (CWT) analysis (Hsu et al., 2003) was used to identify the location of potential source areas of PMF factors and aerosol acidity for each sampling site. CWT combines back-trajectories with measurement data (Seibert et al., 1994; Stohl, 1996) and counts the frequency of back-trajectory endpoints in grid cells that extend over the geographical domain defined by the extension of all trajectories. Then, each grid cell i,j in the domain was used to compute a weighted value obtained by averaging the input variables that have associated trajectories passing the grid cell. CWT was computed for $i \times j$ grid cells of 1° latitude × 1° longitude (approx. 32 × 32 km).

CWT may be affected by the "*trailing effect*," i.e., grid points covered by high numbers of endpoints return statistically stable CWT results, while the results for cells covered by few endpoints may be erroneous. Weighting functions were used to (i) downgrade values of PMF factor contributions in cells where the number of endpoints was less than fixed thresholds, and (ii) remove CWT values for pH and ΔpH in cells for which the number of endpoints is less than 75th percentile. Single CWTs calculated for all the sites were then averaged to obtain the final multiple-site CWT. A weighting function was applied to downgrade values in cells with CWT not calculated at all the single sites. A further smoothing using an isotropic Gaussian kernel with standard deviation 0.75 was performed for better rendering of the results. Details can be found in Section S2.

3. Results and discussion

The European limit value (calculated over 365 days, April 2012-March 2013) of 25 μg m^{-3} was exceeded at 3 sites (PD, RO, VI). The averaged concentration of major analyzed species followed the order (all sites, all seasons, in μg m^{-3}): OM (8.8) > NO$_3^-$ (3.8) > SO$_4^{2-}$ (2.2) > NH$_4^+$ (1.8) > EC (1.3). The spatial patterns for major ions, EC/OC, PAHs and elements are separately discussed in previous publications (Masiol et al., 2015; Khan et al., 2016; 2018; Benetello et al., 2018, respectively). Results of all the analyzed chemical species on a seasonal basis at each site are summarized in Fig. S4.

3.1. Mass closure

The distributions of concentrations of the various $PM_{2.5}$ chemical components and their contribution to the measured $PM_{2.5}$ are shown in Fig. 1. On average (all sites), the measured and reconstructed concentrations differed by 4% for the "base" and 2% for the "sensitivity" test. These differences correspond to 1 and 0.5 μg m^{-3} (Fig. S5). Nonparametric tests (Kruskal-Wallis rank sum test and Wilcoxon rank sum) indicated that measured and reconstructed $PM_{2.5}$ concentrations were not statistically different ($p \gg 0.05$). Slopes of reconstructed versus measured $PM_{2.5}$ were close to unity (0.84–0.9 for the "base" and 0.87–0.94 for the "sensitivity" test) and intercepts were reasonably low (1.4–2.9 μg m^{-3} for the "base" and 1.1–2.7 μg m^{-3} for the "sensitivity" test). The bias in the prediction of the slopes and intercepts was investigated by ordinary nonparametric bootstrap resampling (2000 replicates)
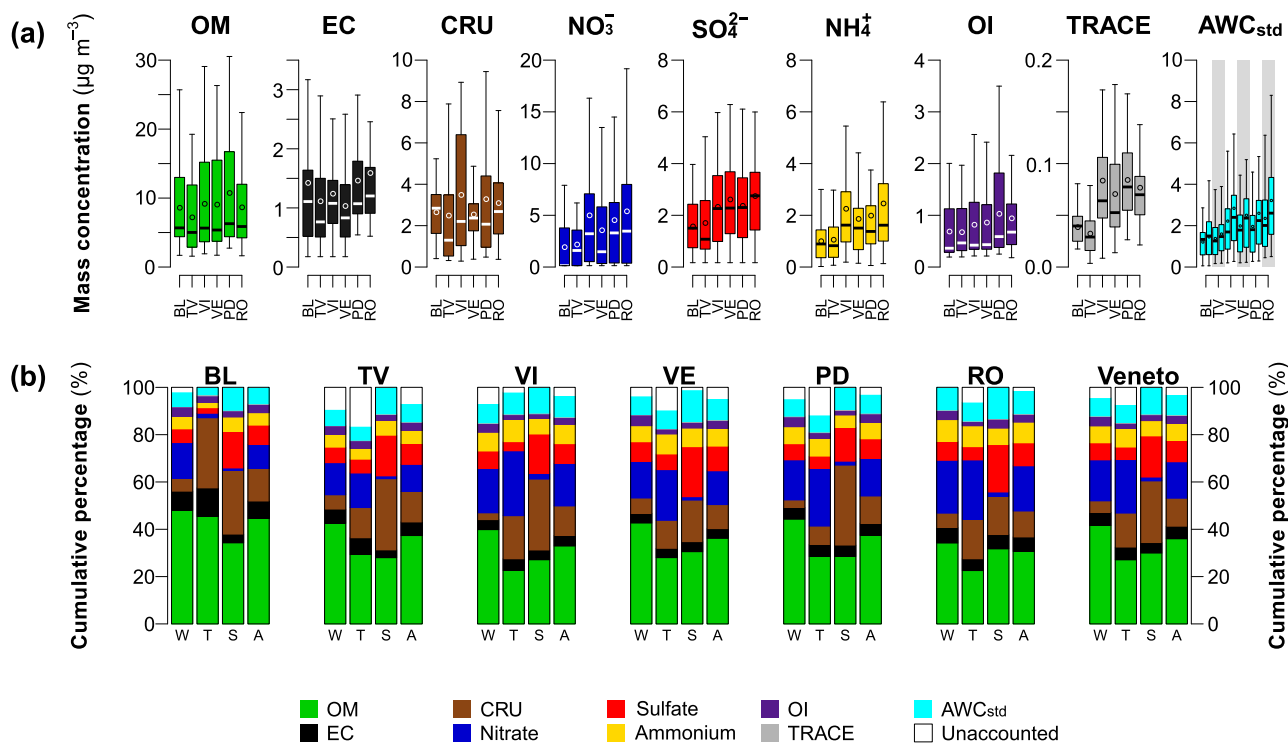
Fig. 1. Results of the hyb-MS-MC approach: (a) boxplot of the annual (all seasons) concentrations of PM2.5 major chemical components modelled at each city, and (b) cumulative percentage of reconstructed PM$_{2.5}$ mass concentrations during the 3 seasons (W = winter; T = transition; S = summer) and during the whole study period (A = annual). Boxplots: line = median, box = inter-quartile range, whiskers = ±1.5*inter-quartile range; outliers and extremes are not shown. For each site, boxplots of AWC$_{std}$ (plot a) are provided for both the "base" and "sensitivity" simulations derived from ISORROPIA-II model, while the "average" are used in the cumulative percentage (plot b).

(Davison and Hinkley, 1997). The slopes (bootstrap average ± standard error) were 0.89 ± 0.01 ("base") and 0.93 ± 0.01 ("sensitivity"), with adjusted bootstrap percentile intervals at 95th confidence level in the 0.86–0.91 and 0.9–0.95 ranges, respectively. The intercepts were estimated as 1.74 ± 0.31 μg m^{-3} ("base") and 1.38 ± 0.3 μg m^{-3} ("sensitivity"), with adjusted bootstrap percentile intervals (α = 0.95) in the 1.2–2.4 μg m^{-3} and 0.8–2 μg m^{-3} ranges, respectively. The reconstructed PM$_{2.5}$ values were able to explain 96% of the measured PM$_{2.5}$ variance for both "base" and "sensitivity" cases.

OM accounted for 31–45% of the average PM$_{2.5}$ mass at all sites, followed by nitrates (10–19%), CRU (10–14%), sulfates (8–10%), water (7–10%), ammonium (5–9%), EC (4–7%), while the remaining components accounted for only 3–4% (Fig. 1b). The Kruskal-Wallis ANOVA on ranks test determined statistically significant differences in the concentrations of the reconstructed chemical components among the sites. Hence, the nonparametric Dunn's tests of multiple comparisons using rank sums showed that the concentrations of chemical components were statistically non-different (p > 0.05) among sites in the Valley (VI, VE, PD, RO), but generally different in BL and TV against the other sites. This result indicates that the PM$_{2.5}$ chemical composition in the cities of the Valley is quite similar. Analyses of covariance were further used for comparing the regression estimates at each site. Results show that the regression slopes across sites were not statistically different (p = 0.67).

The seasonal patterns of the chemical components were similar at all the sites (Fig. S6). Generally, OM, EC, nitrate, ammonium, OI, and TRACE were higher in winter and lower in summer, following the PM$_{2.5}$ mass pattern. CRU had the opposite pattern, likely because resuspension is favored by the drier summer weather conditions. Sulfate had also higher concentrations in summer. Since the SO$_2$ concentrations are relatively constant during the year across the Veneto (Masiol et al., 2017), higher sulfate during summer is likely linked to the enhanced photochemistry favoring the formation of ammonium sulfate (Seinfeld and Pandis, 2016). Enhanced removal during the winter may be also contributing to this seasonal pattern.

3.2. Ambient aerosol water content

In contrast to the AWC$_{std}$ used for mass closure, the AWC computed using the ambient air temperature and RH provides an estimation of aerosol water content under ambient conditions. The annual average ambient air RH ranged from 63% (TV) to 79% (BL, VE). Daily average values were usually higher than 50%. Consequently, AWC was generally higher than AWC$_{std}$.

The annual average AWC for all sites was 19.5 μg m^{-3} with little variation between the base and sensitivity tests (±0.5 μg m^{-3}). Seasonally, AWC followed the pattern of ambient RH (Fig. 2a), i.e. higher concentrations in winter (base-sensitivity annual averages of all sites 36.9–37.2 μg m^{-3}) and lower in summer (2.5 μg m^{-3}). TV had the lower AWC (base-sensitivity annual averages 3.6–4.2 μg m^{-3}), followed by BL (10.5–10.9 μg m^{-3}), while sites in the lower Po Valley showed annual averages ranging from 18.7 to 19.4 μg m^{-3} (PD) to 31–32.4 μg m^{-3} (RO).

The AWC led to an increase of the ambient PM$_{2.5}$ mass by as much as a factor of 3.75 under high RH. On average for all the sites, this increase reached a factor of 1.7. The relationship between total PM$_{2.5}$ including water and ambient RH was further investigated to quantify the increase of PM$_{2.5}$ mass due to AWC in the Veneto region. The increase was exponential by fitting the data with least-squares estimates of the parameters of the nonlinear model (Bates and Chambers, 1992) as:

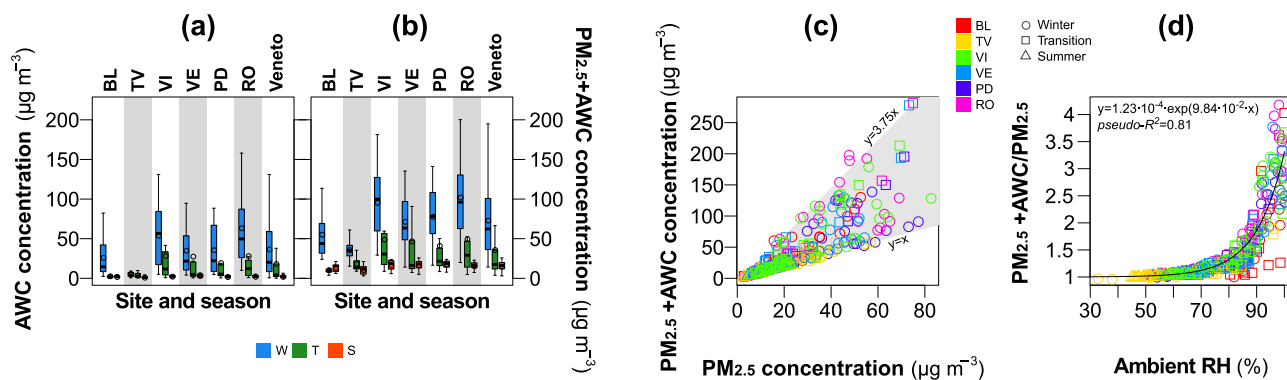$$PM_{2.5} + AWC/PM_{2.5} = a \cdot \exp(b \cdot RH) \qquad (4)$$

Fig. 2. Aerosol water content (AWC) and PM$_{2.5}$ mass concentration corrected for AWC (PM$_{2.5}^{AWC}$) derived from ISORROPIA-II. Boxplots: distribution of estimated AWC (a) and PM$_{2.5}^{AWC}$ (b) at all the single sites and combined (6 cities = Veneto); W = winter, T = transition, S = summer. Scatterplots: (c) relationship between PM$_{2.5}$ measured under standard conditions (48 h conditioning at 20 ± 1 °C and 50 ± 5% RH) and corrected for AWC at ambient air temperature and RH; (d) fit of growing PM$_{2.5}$ mass concentration with RH. Data refer to the "average" results.

where $a = 1.23 \cdot 10^{-4}$, $b = 9.84 \cdot 10^{-2}$. The PM$_{2.5}$ concentration in the region approximately doubles at RH≈92% (16% of sample exceed this RH). This analysis reveals that PM$_{2.5}$ includes a large amount of water during the transition and winter periods. Under these conditions, biomass burning aerosol can undergo chemical changes in the aqueous-phase as previously observed in the Po Valley (Gilardoni et al., 2016).

3.3. Aerosol acidity

The ISORROPIA-II model estimated acidic to moderately acidic aerosol (pH 1.5–4.5, Fig. 3a) with significantly lower pH values in summer (average all sites 2.2) than in winter (3.9) (Kruskal-Wallis ANOVA on Ranks at $p < 0.05$). The variation of pH values between the "base" and "sensitivity" simulations was around ±0.8 pH units in winter and transition, and ±0.5 in summer. Spatially, BL exhibited the highest pH values (annual average 3.6), followed by TV (3.2), and the other sites (3). This finding is related to the higher concentrations of sulfate found in these two sites (Fig. 1a). The pH values are computed from the ionic composition and ISORROPIA-II assuming that particles of all sizes have similar composition in the PM$_{2.5}$ range. Because of this, the pH values reflect an "average" pH of the aerosol over the PM$_{2.5}$ range, i.e. in reality some particles can be more and some less acidic.

A statistically significant linear relationship was found between pH and air temperature for the "base", "sensitivity", and "average" cases (Fig. 3b) with r^2 values in the 0.7–0.91 range. Estimated pH decreased 0.7–0.9 units for each 10 °C increase of ambient air temperature. A moderate relationship was also found with solar

irradiation ($r^2 = 0.5$–0.6, Fig. S7) due to its correlation with air temperature ($r = 0.78$). Temperature has a strong effect on nitrate partitioning as NO$_3^-$ decreases in the aerosol as the temperature rises. The nitrate partitioning shifts AWC and pH from a nitrate-dominated regime to a sulfate-dominated regime. Weak correlations were found with RH ($r = 0.46$–0.59 for the base and sensitivity cases) and AWC ($r = 0.27$–0.31; Fig. 3c,d). The strength of these correlations was likely reduced from the analysis of 24-h integrated samples (and associated noise) not accounting for the wide range of composition and diel variations in association with air temperature and RH patterns.

pH showed a logarithmic relationship ($r^2 = 0.63$) with the sulfate to nitrate ratio (in equivalents) (Fig. 3e). This finding agrees with the chemistry of sulfate- and nitrate-dominated pH regimes discussed by Guo et al. (2017). The reaction of gas-phase ammonia and nitric acid to form ammonium nitrate aerosol is favored at low temperature and high RH typical of wintertime. Ammonium nitrate formation decreases the concentration of H$^+$ in the aerosol aqueous phase increasing pH as the salts formed are less acidic than sulfate (Guo et al., 2016). Conversely, nitric acid is almost completely in the gas-phase in summer (Fig. 1b) allowing for a lower pH dominated by sulfuric acid, ammonium bisulfate and ammonium sulfate.

3.4. Estimated solid- and aqueous-phase aerosol

Even if we assume that the aerosol is metastable, ISORROPIA-II also estimates the presence of solid phase together with the aqueous solution. Sulfate can also be present in the solid-phase as
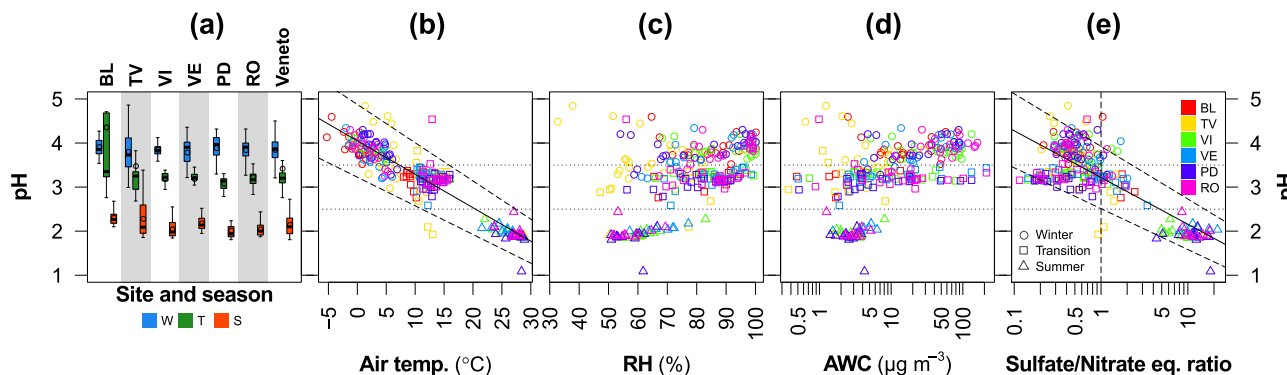

Fig. 3. Aerosol acidity (pH) derived from ISORROPIA-II. Data refer to the "average" results. The boxplot (a) shows the distribution of estimated pH at all the single sites and combined (6 cities = Veneto); W = winter, T = transition, S = summer. Scatterplots show the relationship between pH and average daily air temperature (b), RH (c), AWC (d; modelled by ISORROPIA-II) and sulfate to nitrate ratio equivalent ratio (e). Lines in plot (b) and (e) show linear regressions with pH estimated from the "average" (solid), "base" and "sensitivity" (dotted) simulations.

CaSO$_4$ at ambient temperature and RH conditions. The predicted annual mean concentration of solid-phase CaSO$_4$ ranged from 0.4 μg m^{-3} (BL) to 0.5 μg m^{-3} (other sites) and showed higher concentrations in winter and lower in the transition period at all the sites (Fig. S8a). The solid-phase fraction of sulfate was higher during fall, with annual averages (Fig. S8b) ranging from 17% (RO) to 27% (TV).

Sulfuric acid is a main driver for both pH and AWC. Thus, the "binding" effect of Ca and its impact on pH through the reduction of inorganic aerosol water and H$^+$ were investigated further. Fig. S9 shows the scatterplots between the solid-phase fraction of sulfate and modelled pH with varying AWC and RH segregated into the 3 periods. Statistically significant ($p < 0.05$) linear fits were found in summer ($r^2 = 0.59$) and winter ($r^2 = 0.28$) with a higher slope in summer, indicating an increase of 0.23 pH units for each 10% increase in the solid-phase fraction of sulfate. The effect of Ca is more evident during the summer, i.e. the period with the lower pH that is dominated by ammonium sulfate. The same plot also shows that AWC and RH affected also this relationship: the lower solid-phase fraction of sulfate and higher pH are in agreement with the higher AWC and RH. Similarly, Fig. S10 shows the relationship between the solid-phase fraction of sulfate with the logarithm of AWC. Again, higher r^2 were obtained in summer (0.58), while samples collected in the transition and winter seasons exhibited weaker relationships ($r^2 \approx 0.25$). This result indicates that aerosol water is likely reduced due to the reaction of sulfate with Ca, with this effect being more evident in summer.

3.5. Source apportionment

K$^+$ was selected over total K as a better tracer for biomass burning. Bulk Mg and Ca were included because had less samples below DLs compared to their ionic species. Total sulfur was excluded to avoid double counting given its high correlation with sulfate (r = 0.94). PAH congeners were included as "weak" variables because of the possible artefacts due to the different gas-to-particle partitioning and chemical reactivity during different seasons. The PMF analysis was repeated without PAHs and the results exhibited similar profiles indicating that these semi-volatile species do not drive the model. The variables and their signal-to-noise categories are reported in Table S4.

The optimal solution was found by excluding BL, including 30 (out of original 42) variables, removing only 2 samples, and adding 10% of extra-modeling uncertainty. BL was excluded because it significantly worsened the diagnostics even after constraining the solutions. This result is likely related to the different topography of the territory (Alpine valley) with respect to the other cities as well as the different PM$_{2.5}$ chemical composition previously pointed out by the nonparametric Dunn's tests over the mass closure components. In addition, excluding BL also allowed restricting the PMF results to cities only in the Po Valley. The two excluded samples (one in TV and one in VI) showed very high scaled residuals for some species probably due to construction activities close to the sites or possible sample contamination. The most reasonable solution for the 5 sites in the Po Valley was derived from 298 samples. This solution showed just 3 scaled residuals exceeding ±3, high r^2 (0.94, Fig. S11), the absence of unmapped factors in BS, and minima swaps in DISP. The G-space plots showed no edges. Thus, the effect of FPEAK was investigated but FPEAK was ultimately set to zero. No constraints (Brown et al., 2015) were applied to the final solution after extensive exploration found no improvement in the profiles and a degradation in the fits to certain elements. The six factor profiles are shown in Fig. 4. The annual source contributions and seasonal cumulative fractions of reconstructed mass are reported in Fig. 5.

Two secondary sources were identified. The "secondary nitrate" (SN) source includes most of nitrate (84%) ammonium (54%), and chloride (52%), but also has high shares of elements (Pb, Mn, Zn, Cu; Sb; 18–32%), and OC (18%). The high concentration of chloride is unusual for an ammonium nitrate factor. This factor could represent two distinct sources resulting from a poorly resolved PMF solution due to the similar seasonal variability of nitrate and chloride. However, the chemical profile remains similar for solutions up to 8 factors and does not present swaps with other factors. Reactions of ammonia with both nitric acid and hydrochloric acid forming the corresponding salts in the same periods is another explanation. The secondary sulfate (SS) factor contains sulfate (83%), ammonium (40%), and OC (35%), but also significant amounts of metals (Ba, Ti, Pb; 36–22%), Na$^+$ (25%), and K$^+$ (23%). The two secondary factors include secondary organic aerosol that has condensed on pre-existing particles. Acidic particles may act as cloud condensation nuclei and may also enhance SOA formation (Kleindienst et al., 1999; Zhang et al., 2007; Kroll and Seinfeld, 2008; Hallquist et al., 2009; Kuwata et al., 2015). These two secondary factors are characterized by the highest OC to EC ratios (8.8 and 17.1, respectively) and have negligible contributions to PAHs.

On an annual basis, the highest average concentrations of the secondary nitrate factor ranged between 3.6 μg m^{-3} at TV (21% of PM$_{2.5}$ mass) and 10.6 μg m^{-3} (37% of PM$_{2.5}$ mass) at RO. The average concentration in the 5 sites was 7.7 μg m^{-3} (30% of PM$_{2.5}$ mass). Seasonally, the typical SN pattern was observed across the sites (Figs. S12 and S13), i.e. highest concentrations during colder months and negligible in summer. This pattern was driven by: (i) the more favorable thermodynamic conditions for ammonium nitrate formation at lower temperatures and higher relative humidity (Stelson and Seinfeld, 1982); and (ii) the increase in NO$_x$ emissions due to emissions from space/residential heating.

The average annual concentrations of the secondary sulfate factor varied from 6.7 μg m^{-3} (39%) at TV to 10.3 μg m^{-3} (37%) at RO. The highest sulfate factor concentrations were detected in summer, as a result of the enhanced photochemistry that favors the formation of sulfates (Seinfeld and Pandis, 2016).

The vehicular traffic (TRA) factor is responsible for a significant fraction of transition metals (Cu, Ni, Mn, Fe, Zn; 33–70%), Pb (28%), Sb (50%), Ba (29%), EC (19%), and the OC (16%). Metals can be emitted from exhaust-related sources (fuel and lubricant combustion, catalytic converters, particulate filters, and engine corrosion) as well as from non-exhaust sources (brake and tire wear, muffler ablation) (Pant and Harrison, 2013; Padoan and Amato, 2018; Gustafsson, 2018; Panko et al., 2018; Kukutschová and Filip, 2018). The profile of the factor was characterized by OC/EC≈4 and accounted for 1–5% of PAH congeners. Annually, traffic contributed from 0.5 μg m^{-3} (3%) to 5.8 μg m^{-3} (20%) of PM$_{2.5}$ in TV and PD, respectively. The average contribution over all cities was 2.9 μg m^{-3} that is 12% of the PM$_{2.5}$. The TRA factor exhibited higher contributions during winter (Fig. S12). Since this source is mostly local, the seasonal pattern was likely linked to the lower mixing layer heights and lower wind speeds in winter and the consequent buildup of primary air pollutants.

The factor responsible for a significant fraction of the crustal elements (Al, Mg, Ca, Ti, Ba; 21–97%) and EC (17%) was interpreted as re-suspended dust (RD). Road surfaces consist of a mixture of geological materials with bitumen, and modifiers such as fillers and adhesives (Thorpe and Harrison, 2008). Particles from multiple sources also deposit on road surfaces and may be resuspended (Amato et al., 2014; Padoan and Amato, 2018; Kukutschová and Filip, 2018; Panko et al., 2018; Gustafsson, 2018; Denby et al., 2018). In addition, other sources present in urban areas, such as construction activities, can contribute to this factor. Although the DISP ranges showed high variability in the profile for OC, this
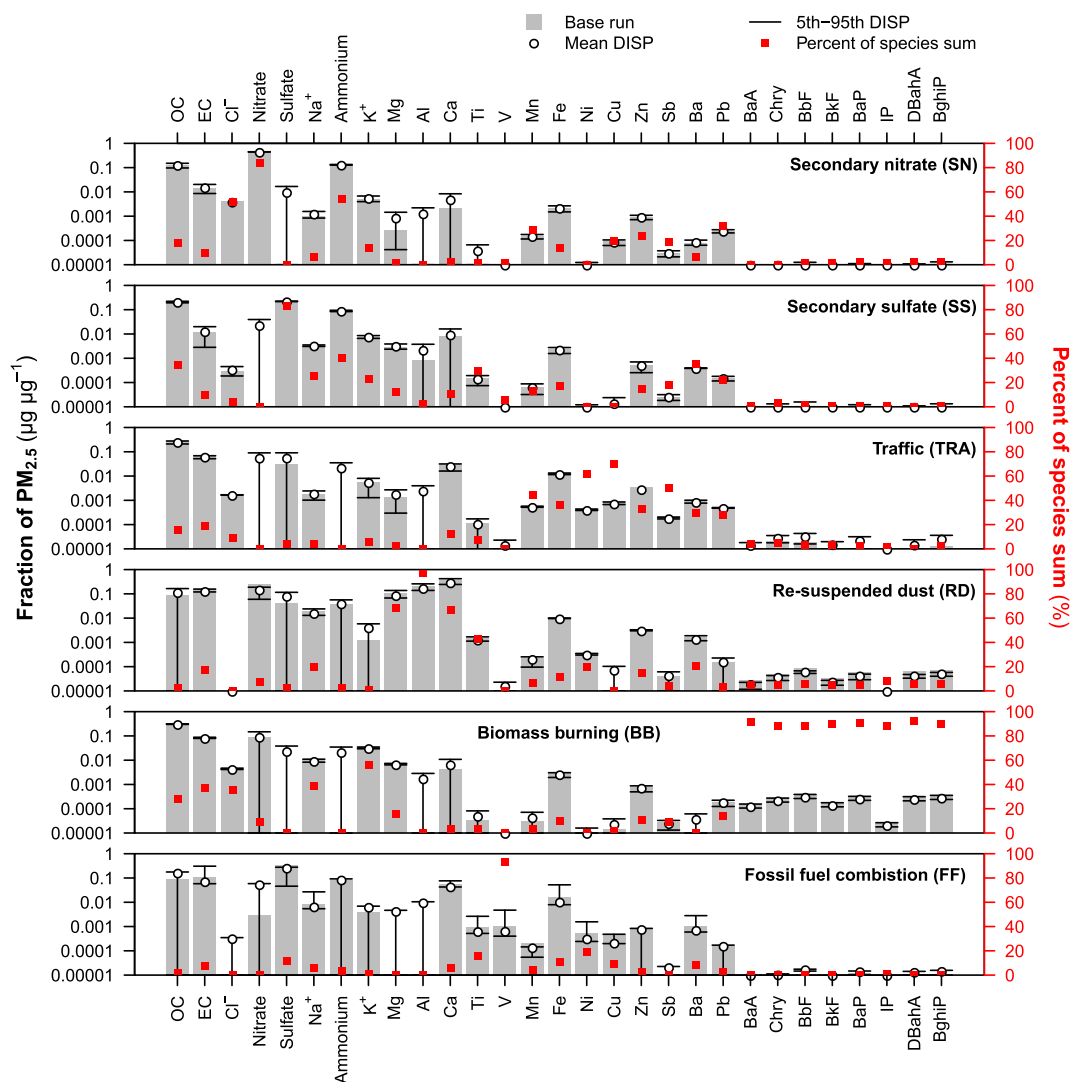
Fig. 4. Multiple-site PMF factor profiles. Left y-axis: bars represent mass contribution of base run, open circles represent the mean DISP values with the error bars providing the range (minima and maxima values) of DISP values. Right y-axis: red filled squares show factor contributions in percent of species sum. (For interpretation of the references to colour in this figure legend, the reader is referred to the web version of this article.)

source accounts for more EC than OC in mass contribution with the lower OC/EC ratio (0.6) among the factors. This factor contributes 5–8% of PAH congeners, i.e. apparently more than TRA. However, the difference between the two factor profiles for PAHs is almost negligible when accounting for the upper DISP ranges, as statistically tested using the Kruskal-Wallis ANOVA on ranks at $p < 0.05$. RD contributed about 4–6% of $PM_{2.5}$ in all the cities, ranging from 0.9 μg m^{-3} (TV) to 1.7 μg m^{-3} (RO) on an annual basis. Generally, RD factor concentrations were higher in spring and summer (Fig. S12), possibly due to the drier weather conditions favoring the resuspension from soil and road surfaces. However, the patterns of the daily concentrations were different among sites (Fig. S13), likely indicating that this is a local source. The BB factor includes a high percentage of the measured K$^+$ (56%), a major tracer for this source, as well as other ions (Na$^+$ 39%, Cl$^-$ 35%, nitrate 9%), EC (38%), OC (28%), and accounts for most of PAH congeners (88–92%). Similar to the secondary nitrate, this factor was further investigated for being the result of a poorly resolved PMF solution also including sea-salt aerosol or road salt. However, the chemical profile remains similar for solutions up to 8 factors and did not present swaps with any other factor indicating its stability. There is little or no sulfate in this factor (DISP range 0–3%). The OC/EC ratio in the

factor profile was 3.6. BB annual contribution to $PM_{2.5}$ varied from 2.9 μg m^{-3} (10%) in RO to 5.8 μg m^{-3} (34%) of $PM_{2.5}$ in RO and TV (average over all cities: 4.4 μg m^{-3}, 17%). The BB factor exhibited higher concentrations in winter at all sites (Fig. S12) due to the emissions from residential wood combustion, while it was always less than 0.2 μg m^{-3} in summer (Belis et al., 2011; Piazzalunga et al., 2013; Pietrogrande et al., 2015; Benetello et al., 2017).

The last factor reflects the fossil fuel (FF) combustion. It explains most of vanadium (93%) and includes high percentages of Ni (19%), Ti (16%), and sulfate (11%). V and Ni are usually associated with the petrochemical industry (Bosco et al., 2005; de la Campa et al., 2011), residual oil combustion (Moreno et al., 2010), coke production (Moreno et al., 2007), and shipping emissions (Moldanová et al., 2009; Becagli et al., 2012). Most of these potential sources are present in the industrial area of Porto Marghera, close to Venice-Mestre. Similar factors were previously reported in Venice-Mestre in PM_{10} (Masiol et al., 2012), $PM_{2.5}$ (Masiol et al., 2014), and PM_1 (Squizzato et al., 2016) even if the V-Ni relationship is usually stronger in the coarse particles than in the fine particles (Moreno et al., 2007). FF accounted for 0.1 μg m^{-3} (1%) in TV, 0.7–1 2 μg m^{-3} (3–4%) in VI, PD, RO, and reached 1.2 μg m^{-3} (5%) in VE. The higher contribution found in VE was probably related to
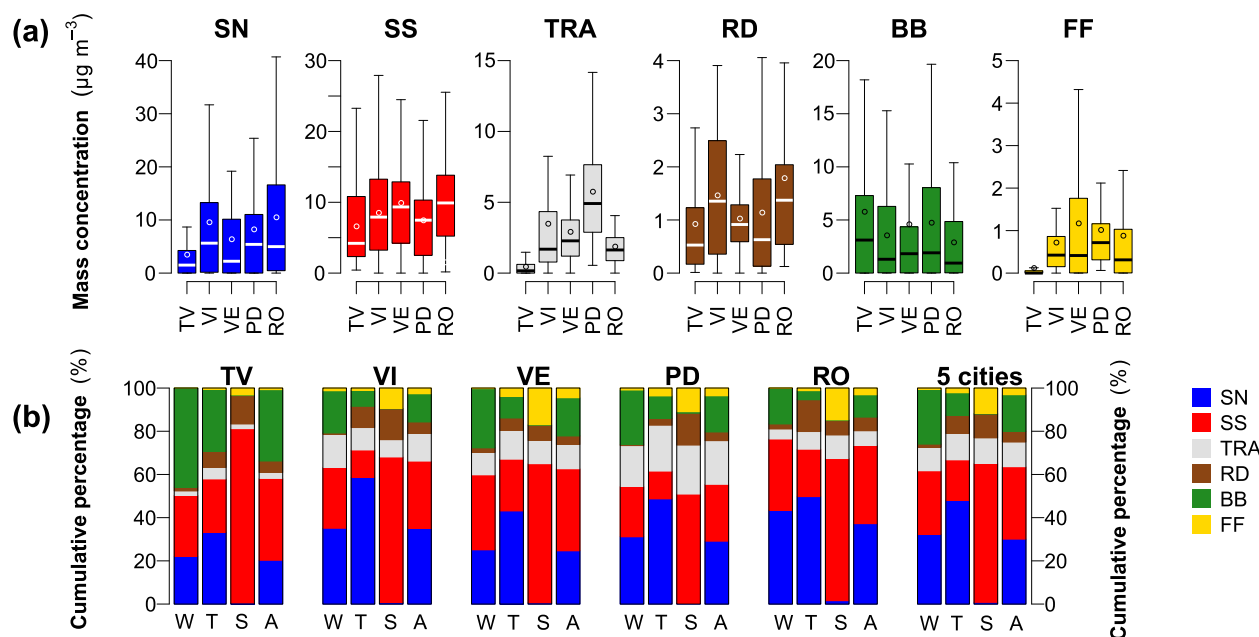
Fig. 5. Results of the multiple-site PMF: (a) boxplot of the source contributions at annual basis (all seasons), and (b) cumulative percentage of reconstructed PM$_{2.5}$ mass concentrations during the 3 seasons (W = winter; T = transition; S = summer) and during the whole study period (A = annual). Boxplots: line = median, box = inter-quartile range, whiskers = ±1.5*inter-quartile range; outliers and extremes are not shown. Sources: SN = secondary nitrate; SS = secondary sulfate; TRA = traffic; RD = re-suspended dust; BB = biomass burning; FF = fossil fuel combustions.

the additional emissions from cargo and cruise ships. FF showed higher contributions in summer (Fig. S12). This pattern could be driven by the peak in energy production from coal power plants and more intense ship traffic in the cruise harbor in VE. Despite the clear seasonal patterns of the contributions of FF factor and the concentrations of vanadium (Fig. S4), the Ni/V diagnostic ratio (Fig. S14) did not show any seasonal pattern or any difference among sites. Thus, the Ni/V diagnostic ratio cannot be used to extract more information about the type of combustion source.

Although a marine aerosol factor can be expected (mainly in the coastal city, VE), PMF analysis did not identify a clear sea-salt source. This result agrees with the literature. Studies using receptor modeling in the Easter part of the Po Valley have detected sea-salt factors only in PM$_{10}$ (Venice area: Masiol et al., 2012; Bologna: Tositti et al., 2014), but not in PM$_{2.5}$ (Venice area: Masiol et al., 2014; Treviso: Squizzato et al., 2017).

3.6. Source-specific contributions to AWC and aerosol acidity

Stepwise regression analyses adopting the Akaike information criterion as an estimator of the relative quality of statistical models were performed to investigate the relationship between the estimated pH, ΔpH, AWC and ΔAWC (each one as dependent variable) and the PMF source contributions (independent variables). The regressions using the "deltas" reduce the impact of temperature, RH, and seasonality (Shi et al., 2017). Conversely, regressions with pH and AWC include the seasonal variability of T and RH also accounting for the seasonal differences in the aerosol composition. The measure of predictive ability for multiple linear regression with variables selected by the stepwise process was assessed using the k-fold cross-validation (Braun and Maindonald, 2010; James et al., 2013). The k-fold method randomly partitions the original dataset into k (k = 10, in this case) equal-sized subsamples and recursively uses k-1 parts to re-fit the regression and 1 part as a testing set. The cross-validation root mean squared error was used as a quantitative measure of error associated to the estimates. In addition, the

R^2_{adj} shrinkage was assessed via k-fold cross-validation to return a cross-validated adjusted coefficient of determination (Table 1).

Similar results were obtained for both pH and ΔpH using the estimation of the "base", "average" and "sensitivity" simulations (Table 1). However, better fits were obtained for pH (adjusted R^2 = 0.67–0.74) than for ΔpH (0.25–0.58). Conversely, ΔAWC shows higher R^2_{adj} (0.61–0.62) than AWC (0.54).

Both pH and ΔpH were affected more by the nitrate, biomass burning (increase) and sulfate and fossil fuel combustion (decrease) factors. The nitrate factor also drives the source dependence of both AWC and ΔAWC. These results are consistent with those reported by Shi et al. (2019) in China. The positive correlation between SN and pH is related to the fact that nitrate formation is favored at higher pH values (Guo et al., 2017). There is also a significant positive association between the SN factor and AWC and ΔAWC (Table 1). The negative effect of SS and FF factors on pH and ΔpH was related to their chemical fingerprint as both carry high loadings of sulfate. Shi et al. (2019) reported a similar behavior. SS was negatively correlated with pH during summertime when the increased temperatures and lower RH lead to a decrease of the aerosol water and to a subsequent increase of H$^+$ concentration. Similarly, in Veneto, the highest sulfate concentrations were recorded during summertime and it is likely that part of that sulfate is ammonium bisulfate.

3.7. Potential effect of regional transport

The potential effect of regional transport on PM$_{2.5}$ and acidity was investigated using a multiple-site concentration-weighted trajectory analysis. Fig. 6 reports the resulting maps for the factors more affected by transport as well as for pH and ΔpH. Air masses coming from Central and Eastern Europe were associated with the increased nitrate, sulfate, and biomass burning factors as well as pH. This pattern was previously observed by Squizzato and Masiol (2015) considering only a Venice site during winter. High concentrations of sulfate factor were observed when air masses come from Eastern Europe, where there are significant sources of

Table 1
Results of the stepwise regressions between pH, ΔpH (dependent variable) and the PMF source contributions (independent variables). Regressions are repeated using the pH and ΔpH values computed with ISORROPIA-II for the "base", "average", and "sensitivity" simulations. The table reports the coefficients of the regressions (β) and the β multiplied for the average independent variables over the whole study period ($\beta \cdot \overline{C}$). Sources: SN = secondary nitrate; SS = secondary sulfate; TRA = traffic; RD = re-suspended dust; BB = biomass burning; FF = fossil fuel combustion.

pH	Model	Intercept	SN	SS	TRA	RD	BB	FF	R^2_{adj}	CV-RMSE	CV-R^2_{adj}
β	"base"	2.000	0.024	−0.007	0.012	0.039	0.064	−0.124	0.67	0.415	0.65
	"average"	2.786	0.026	−0.019	–	–	0.076	−0.151	0.74	0.410	0.73
	"sensitivity"	3.485	0.028	−0.030	–	–	0.089	−0.176	0.73	0.477	0.72
$\beta \cdot \overline{C}$	"base"	2.000	0.188	−0.063	0.034	0.050	0.279	−0.099	0.67	–	0.65
	"average"	2.786	0.203	−0.163	–	–	0.333	−0.121	0.74	–	0.73
	"sensitivity"	3.485	0.219	−0.264	–	–	0.388	−0.141	0.73	–	0.72
ΔpH	**Model**										
β	"base"	−0.192	0.006	–	–	0.036	0.029	−0.053	0.25	0.382	0.21
	"average"	−0.115	0.006	−0.010	–	0.019	0.030	−0.064	0.43	0.272	0.37
	"sensitivity"	−0.022	0.006	−0.022	–	–	0.031	−0.073	0.58	0.237	0.43
$\beta \cdot \overline{C}$	"base"	−0.192	0.048	–	–	0.046	0.127	−0.043	0.25	–	0.21
	"average"	−0.115	0.044	−0.086	–	0.025	0.132	−0.052	0.43	–	0.37
	"sensitivity"	−0.022	0.043	−0.191	–	–	0.137	−0.058	0.58	–	0.43
AWC	**Model**	**Intercept**	**SN**	**SS**	**TRA**	**RD**	**BB**	**FF**	R^2_{adj}	**CV-RMSE**	**CV-R^2_{adj}**
β	"base"	−3.786	2.235	–	1.051	–	0.490	2.095	0.54	24.4	0.51
	"average"	−3.099	2.263	–	1.063	–	0.434	1.957	0.54	24.4	0.52
	"sensitivity"	0.049	2.275	–	1.348	–	–	–	0.54	24.5	0.52
$\beta \cdot \overline{C}$	"base"	−3.786	17.913	–	3.188	–	2.149	1.728	0.54	–	0.51
	"average"	−3.099	18.137	–	3.224	–	1.903	1.614	0.54	–	0.52
	"sensitivity"	0.049	18.230	–	4.087	–	–	–	0.54	–	0.52
ΔAWC	**Model**										
β	"base"	−10.163	1.712	–	–	–	–	3.462	0.61	15.0	0.58
	"average"	−10.409	1.722	–	–	–	–	3.430	0.61	14.9	0.58
	"sensitivity"	−10.654	1.733	–	–	–	–	3.398	0.62	14.9	0.61
$\beta \cdot \overline{C}$	"base"	−10.163	13.720	–	–	–	–	2.855	0.61	–	0.58
	"average"	−10.409	13.803	–	–	–	–	2.829	0.61	–	0.58
	"sensitivity"	−10.654	13.887	–	–	–	–	2.802	0.62	–	0.61

SO₂ (EEA, 2019), while SO₂ concentrations in Veneto were well below the lower assessment threshold for vegetation protection during the whole year (Masiol et al., 2017). Alternatively, the highest NO₂ concentrations, the main precursor of PM nitrate, were recorded in Northern Italy, Germany, and Eastern Europe countries (EEA, 2019).

The regional contributions to the biomass burning factor can be related both to wildfires and residential biomass burning (wood, wood chips, and wood pellets) in Central and Northern Europe. Germany, France, and Poland are top countries in Europe for wood chips consumption. In addition, Germany, Denmark, and Austria are amongst the largest consumers of wood pellets for heating
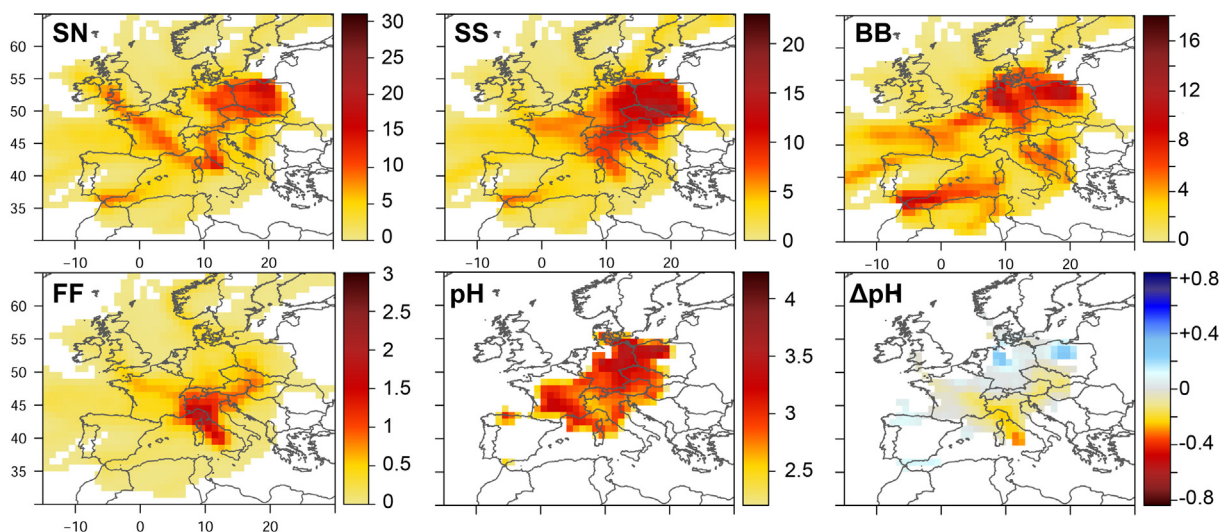

Fig. 6. Results of the MS-CWT analysis. Sources: SN = secondary nitrate; SS = secondary sulfate; BB = biomass burning; FF = fossil fuels combustion. Units are expressed in μg m−3 for sources; pH units for pH and ΔpH. Transparent pixels denote endpoints not meeting the criteria in the weighting functions.

(AEBIOM, 2015). The high contribution to the fossil fuel combustion factor from North and Central Italy can be attributed to the emissions from coal and oil-fired power plants and from waste incinerators located in these areas (CarbonBrief, 2019; Global Energy Observatory, 2019).

Regional transport affected both pH and ΔpH. The pH map suggests contributions of the sources in Central and Eastern Europe, while the ΔpH shows positive contributions from Germany and Poland and negative contributions from Northern Italy and the Mediterranean area. Generally, less acidic aerosol was present when air masses come from the North and probably linked to the higher concentrations of nitrate factor that had a positive effect on the pH. The more acidic particles were present when the air originated in the Tyrrhenian Sea area and were likely related to the fossil fuel source (FF and ΔpH have similar spatial patterns; Fig. 6). The loss of fine nitrate due to reaction with larger sea-salt particles may also contribute to lower the fine PM ΔpH.

4. Conclusions

This study integrates various tools to investigate the $PM_{2.5}$ chemical composition, sources, acidity, aerosol water content, and their relationships across a European air pollution hotspot.

The combination of the traditional mass closure approach with the inorganic aerosol water content estimated by a thermodynamic model help to better reconstruct the absolute $PM_{2.5}$ mass concentration. The hybrid mass closure approach showed that the concentrations of the reconstructed chemical components were statistically non-different among sites in the Valley, suggesting a quite homogeneous $PM_{2.5}$ chemical composition in the lower end of the Po Valley. At all sites, organic matter represented 31–45% of the $PM_{2.5}$ mass followed by nitrate (10–19%), crustal material (10–14%), sulfate (8–10%), ammonium (5–9%), elemental carbon (4–7%), other inorganic ions and trace elements (3–4%).

The all-site average $PM_{2.5}$ inorganic water content at ambient conditions was 19.5 μg m^{-3} with significantly higher concentrations in winter (following the pattern of ambient RH). The increased $PM_{2.5}$ mass due to the aerosol water showed an exponential relationship with RH, increasing on average by a factor of 1.7 the ambient $PM_{2.5}$ mass concentration.

A multiple-site receptor model performed over 5 cities indicated that the lower end of the Po Valley is affected by 6 main sources with similar profiles across the region. The largest contributor to $PM_{2.5}$ mass was the secondary sulfate factor (average 34%) followed by a secondary nitrate factor (30%), biomass burning (17%), traffic (11%), re-suspended dust (5%), and fossil fuel combustions (3%). Biomass burning accounted for ~ 90% of total PAHs.

The $PM_{2.5}$ was generally acidic to moderately acidic (pH 1.5–4.5) throughout the year with lower pH in summer. Estimated pH decreased 0.7–0.9 units for each 10 °C increase of ambient air temperature at all the sites. Aerosol acidity was mostly driven by secondary sulfate, fossil fuel combustions (decreasing pH), secondary nitrate and biomass burning (increasing pH). Secondary nitrate was also found to be the main driver of the aerosol water content.

$CaSO_4$ was the only salt estimated to exist in the solid "metastable" form under ambient conditions. Calcium "binding" sulfate to form $CaSO_4$ had an impact on pH through the reduction of inorganic aerosol water and H^+ with an increase of 0.23 pH units for each 10% increase in the solid-phase fraction of sulfate.

The application of a trajectory ensemble method showed similar results over the 5 sites in the Po Valley. Eastern and Central Europe were the main source areas of the secondary aerosol components. Less acidic aerosol was found when air masses come from Northern Europe due to higher contributions of the nitrate factor. More acidic particles were present when air masses passed over the Po Valley and the Tyrrhenian Sea possibly due to the higher contributions of fossil fuel combustion source and less available fine nitrate aerosol due to interactions with coarse sea-salt particles.

Disclaimer

The views and conclusions expressed in this paper are exclusively of the authors and may not reflect those of ARPAV.

Declaration of Competing Interest

The authors declare that they have no known competing financial interests or personal relationships that could have appeared to influence the work reported in this paper.

Appendix A. Supplementary data

Supplementary data to this article can be found online at https://doi.org/10.1016/j.scitotenv.2019.135287.

References

AEBIOM (European Biomass Association), 2015. AEBIOM Statistical Report 2015, European Bioenergy Outlook, Key Findings 2015. Brussels, Belgium. Available at: http://www.aebiom.org/wp-content/uploads/2015/10/AEBIOM-Statistical-Report-2015_Key-Findings1.pdf (last access on July 2019).

Amato, F., Cassee, F.R., van der Gon, H.A.D., Gehrig, R., Gustafsson, M., Hafner, W., Harrison, R.M., Jozwicka, M., Kelly, F.J., Moreno, T., Prevot, A.S., 2014. Urban air quality: the challenge of traffic non-exhaust emissions. J. Hazard. Mater. 275, 31–36.

ARPAV (Agenzia Regionale per la Prevenzione e Protezione Ambientale del Veneto), 2016. Campagne di monitoraggio di ammoniaca in aria in siti di fondo urbano e presso alcuni allevamenti di bovini e di ovaiole. [in Italian] available at: http://www.arpa.veneto.it/temi-ambientali/aria/file-e-allegati/documenti/concentrazioni-di-ammoniaca-nellaria/Campagne_NH3_2015-2016.pdf (last access on March 2019).

Bates, D.M., Chambers, J.M., 1992. Nonlinear models. In: Chambers, J.M., Hastie, T.J., (Eds.), Statistical Models in S, Wadsworth & Brooks/Cole.

Becagli, S., Sferlazzo, D.M., Pace, G., Sarra, A.D., Bommarito, C., Calzolai, G., Ghedini, C., Lucarelli, F., Meloni, D., Monteleone, F., Severi, M., 2012. Evidence for heavy fuel oil combustion aerosols from chemical analyses at the island of Lampedusa: a possible large role of ships emissions in the Mediterranean. Atmos. Chem. Phys. 12 (7), 3479–3492.

Belis, C.A., Cancelinha, J., Duane, M., Forcina, V., Pedroni, V., Passarella, R., Tanet, G., Douglas, K., Piazzalunga, A., Bolzacchini, E., Sangiorgi, G., 2011. Sources for PM air pollution in the Po Plain, Italy: I. Critical comparison of methods for estimating biomass burning contributions to benzo (a) pyrene. Atmos. Environ. 45 (39), 7266–7275.

Belis, C.A., Larsen, B.R., Amato, F., El Haddad, I., Favez, O., Harrison, R.M., Hopke, P.K., Nava, S., Paatero, P., Prévôt, A., Quass, U., Vecchi, R., Viana, M., 2014. European Guide on Air Pollution Source Apportionment with Receptor Models. JRC Reference Reports EUR26080 EN.

Benetello, F., Squizzato, S., Hofer, A., Masiol, M., Khan, M.B., Piazzalunga, A., Fermo, P., Formenton, G.M., Rampazzo, G., Pavoni, B., 2017. Estimation of local and

external contributions of biomass burning to PM2.5 in an industrial zone included in a large urban settlement. Environ. Sci. Pollut. Res. 24 (2), 2100–2115.

Benetello, F., Squizzato, S., Masiol, M., Khan, M.B., Visin, F., Formenton, G.M., Pavoni, B., 2018. A procedure to evaluate the factors determining the elemental composition of PM2.5. Case study: the Veneto region (Northeastern Italy). Environ. Sci. Pollut. Res. 25, 3823–3839.

Birch, M.E., Cary, R.A., 1996. Elemental carbon-based method formonitoring occupational exposures to particulate diesel exhaust. Aerosol Sci. Technol. 25, 221–241.

Bosco, M.L., Varrica, D., Dongarra, G., 2005. Case study: inorganic pollutants associated with particulate matter from an area near a petrochemical plant. Environ. Res. 99, 18–30.

Bougiatioti, A., Nikolaou, P., Stavroulas, I., Kouvarakis, G., Weber, R., Nenes, A., Kanakidou, M., Mihalopoulos, N., 2016. Particle water and pH in the eastern Mediterranean: source variability and implications for nutrient availability. Atmos. Chem. Phys. 16 (7), 4579–4591.

Braun, W.J., Maindonald, J., 2010. Data Analysis and Graphics Using R: An Example-based Approach (3rd Edition). Cambridge University Press.

Brown, S.G., Eberly, S., Paatero, P., Norris, G.A., 2015. Methods for estimating uncertainty in PMF solutions: examples with ambient air and water quality data and guidance on reporting PMF results. Sci. Total Environ. 518, 626–635.

Canty, A., Ripley, B., 2017. boot: Bootstrap R (S-Plus) Functions. R package version 1.3-20. Available at: https://CRAN.R-project.org/package=boot (last access on July 2019).

CarbonBrief, 2019. Mapped: The world's coal power plants. Available at: https://www.carbonbrief.org/mapped-worlds-coal-power-plants (last access on June 2019).

Carbone, C., Decesari, S., Mircea, M., Giulianelli, L., Finessi, E., Rinaldi, M., Fuzzi, S., Marinoni, A., Duchi, R., Perrino, C., Sargolini, T., 2010. Size-resolved aerosol chemical composition over the Italian Peninsula during typical summer and winter conditions. Atmos. Environ. 44 (39), 5269–5278.

Carslaw, D.C., Ropkins, K., 2012. Openair—an R package for air quality data analysis. Environ. Modell. Software 27, 52–61.

Chow, J.C., Lowenthal, D.H., Chen, L.W.A., Wang, X., Watson, J.G., 2015. Mass reconstruction methods for PM2.5: a review. Air Qual. Atmos. Health 8, 243–263.

Colette, A., Granier, C., Hodnebrog, Jakobs, H., Maurizi, A., Nyiri, A., Bessagnet, B., D'Angiola, A., D'Isidoro, M., Gauss, M., Meleux, F., Memmesheimer, M., Mieville, A., Roüil, L., Russo, F., Solberg, S., Stordal, F., Tampieri, F., Hodnebrog Øand Jakobs, H., Maurizi, A., Nyiri, A., Bessagnet, B., D'Angiola, A., D'Isidoro, M., Gauss, M., Meleux, F., Memmesheimer, M., Mieville, A., Roüil, L., Russo, F., Solberg, S., Stordal, F., Tampieri, F., 2011. Air quality trends in Europe over the past decade: a first multi-model assessment. Atmos. Chem. Phys. 11, 11657–11678.

Colette, A., Aas, W., Banin, L., Braban, C.F., Ferm, M., Gonzalez Ortiz, A., Ilyin, I., Mar, K., Pandolfi, M., Putaud, J.P., Shatalov, V., et al., 2016. Air pollution trends in the EMEP region between 1990 and 2012. EMEP/CCC-Report 1/2016, available at: http://www.nilu.no/projects/ccc/reports/cccr1-2016.pdf (last access on January 2019).

Crippa, M., Janssens-Maenhout, G., Dentener, F., Guizzardi, D., Sindelarova, K., Muntean, M., Van Dingenen, R., Granier, C., 2016. Forty years of improvements in European air quality: regional policy-industry interactions with global impacts. Atmos. Chem. Phys. 16, 3825–3841.

Davison, A.C., Hinkley, D.V., 1997. Bootstrap Methods and Their Applications. Cambridge University Press, Cambridge.

de la Campa, A.S., Moreno, T., De La Rosa, J., Alastuey, A., Querol, X., 2011. Size distribution and chemical composition of metalliferous stack emissions in the San Roque petroleum refinery complex, southern Spain. J. Hazard. Mater. 190 (1–3), 713–722.

Denby, B.R., Kupiainen, K.J., Gustafsson, M., 2018. In: Review of Road Wear Emissions. In Non-Exhaust Emissions. Academic Press, pp. 183–203.

Ding, J., Zhao, P., Su, J., Dong, Q., Du, X., Zhang, Y., 2019. Aerosol pH and its driving factors in Beijing. Atmos. Chem. Phys. 19, 7939–7954.

Dinno, A., 2017. dunn.test: Dunn's Test of Multiple Comparisons Using Rank Sums. R package version 1.3.5. Available at: https://CRAN.R-project.org/package=dunn.test (last access on July 2019).

EEA (European Environmental Agency), 2014. Air quality in Europe – 2014 report. Luxembourg: Publications Office of the European Union. Available at: https://doi.org/10.2800/2277 (last access on March 2019).

EEA (European Environmental Agency), 2016. Air quality in Europe – 2016 report. Luxembourg: Publications Office of the European Union. Available at: https://doi.org/10.2800/80982 (last access on March 2019).

EEA (European Environmental Agency), 2018. Air quality in Europe – 2018 report. EEA Report No 12/2018, Available at: https://doi.org/10.2800/777411 (last access on March 2019).

EEA (European Environment Agency), 2019. Air quality statistics. Available at: https://www.eea.europa.eu/data-and-maps/dashboards/air-quality-statistics (last access on June 2019).

Fang, T., Guo, H., Zeng, L., Verma, V., Nenes, A., Weber, R.J., 2017. Highly acidic ambient particles, soluble metals, and oxidative potential: a link between sulfate and aerosol toxicity. Environ. Sci. Technol. 51 (5), 2611–2620.

Fountoukis, C., Nenes, A., 2007. ISORROPIA II: a computationally efficient thermodynamic equilibrium model for $K^+–Ca^{2+}–Mg^{2+}–NH_4^+–Na^+–SO_4^{2-}–NO_3^-–Cl^-–H_2O$ aerosols. Atmos. Chem. Phys. 7 (17), 4639–4659.

Fox, J., Weisberg, S., 2011. An R Companion to Applied Regression. Sage, Thousand Oaks CA.

Gama, J., 2016. NISTunits: Fundamental Physical Constants and Unit Conversions from NIST. R package version 1.0.1. https://CRAN.R-project.org/package=NISTunits.

Giannouli, M., Kalognomou, E.-A., Mellios, G., Moussiopoulos, N., Samaras, Z., Fiala, J., 2011. Impact of European emission control strategies on urban and local air quality. Atmos. Environ. 45, 4753–4762.

Gilardoni, S., Massoli, P., Paglione, M., Giulianelli, L., Carbone, C., Rinaldi, M., Decesari, S., Sandrini, S., Costabile, F., Gobbi, G.P., Pietrogrande, M.C., 2016. Direct observation of aqueous secondary organic aerosol from biomass-burning emissions. Proc. Natl. Acad. Sci. 113 (36), 10013–10018.

Global Energy Observatory, 2019. Current List of Oil Power Plants. Available at: http://globalenergyobservatory.org/list.php?db=PowerPlants&type=Oil (last access on June 2019).

Grolemund, G., Wickham, H., 2011. Dates and times made easy with lubridate. J. Stat. Softw. 40 (3), 1–25.

Guo, H., Xu, L., Bougiatioti, A., Cerully, K.M., Capps, S.L., Hite Jr, J.R., Carlton, A.G., Lee, S.H., Bergin, M.H., Ng, N.L., Nenes, A., 2015. Fine-particle water and pH in the southeastern United States. Atmos. Chem. Phys. 15 (9), 5211–5228.

Guo, H., Sullivan, A.P., Campuzano-Jost, P., Schroder, J.C., Lopez-Hilfiker, F.D., Dibb, J. E., Jimenez, J.L., Thornton, J.A., Brown, S.S., Nenes, A., Weber, R.J., 2016. Fine particle pH and the partitioning of nitric acid during winter in the northeastern United States. J. Geophys. Res.: Atmos. 121 (17).

Guo, H., Weber, R.J., Nenes, A., 2017. High levels of ammonia do not raise fine particle pH sufficiently to yield nitrogen oxide-dominated sulfate production. Sci. Rep. 7 (1), 12109.

Gustafsson, M., 2018. Review of road wear emissions: a review of road emission measurement studies: identification of gaps and future needs. In: Amato, F., (Ed.) Non-Exhaust Emissions (pp. 161-181), Academic Press.

Hallquist, M., Wenger, J.C., Baltensperger, U., Rudich, Y., Simpson, D., Claeys, M., Dommen, J., Donahue, N.M., George, C., Goldstein, A.H., Hamilton, J.F., 2009. The formation, properties and impact of secondary organic aerosol: current and emerging issues. Atmos. Chem. Phys. 9, 5155–5236.

Hand, J.L., Malm, W.C., 2007. Review of the IMPROVE equation for estimating ambient light extinction coefficients. CIRA, Colorado State University. Available at: http://vista.cira.colostate.edu/improve/Publications/GrayLit/016_IMPROVEeqReview/IMPROVEEquationReview.pdf (last access on July 2019).

Harrell, F.E. Jr., Dupont, C., et al., 2018. Hmisc: Harrell Miscellaneous. R package version 4.1-1. Available at: https://CRAN.R-project.org/package=Hmisc (last access on July 2019).

Harrison, R.M., Jones, A.M., Lawrence, R.G., 2003. A pragmatic mass closure model for airborne particulate matter at urban background and roadside sites. Atmos. Environ. 37, 4927–4933.

Hopke P.K., 2015a. Reactive Ambient Particles. In: Nadadur, S.S., Hollingsworth, J. W., (Eds.) Air Pollution and Health Effects (pp 1-24), Springer, London.

Hopke, P.K., 2015b. Applying multivariate curve resolution to source apportionment of the atmospheric aerosol. ACS Symp. Ser. 1199, 129–157.

Hopke, P.K., 2016. Review of receptor modeling methods for source apportionment. J. Air Waste Manag. Assoc. 66, 237–259.

Hsu, Y.K., Holsen, T.M., Hopke, P.K., 2003. Comparison of hybrid receptor models to locate PCB sources in Chicago. Atmos. Environ. 37, 545–562.

Ito, A., Myriokefalitakis, S., Kanakidou, M., Mahowald, N., Scanza, R., Hamilton, D., Baker, A., Jickells, T., Sarin, M., Bikkina, S., Gao, Y., Shelley, R., Buck, C., Landing, W., Bowie, A., Perron, M., Guieu, C., Meskhidze, N., Johnson, M., Feng, Y., Kok, J., Nenes, A., Duce, R., 2019. Pyrogenic iron: the missing link to high iron solubility in aerosols. Science. Advances 5, eaau7671.

James, G., Witten, D., Hastie, T., Tibshirani, R., 2013. An Introduction to Statistical Learning. Springer, New York.

Kalnay, E., Kanamitsu, M., Kistler, R., Collins, W., Deaven, D., Gandin, L., Iredell, M., Saha, S., White, G., Woollen, J., Zhu, Y., Chelliah, M., Ebisuzaki, W., Higgins, W., Janowiak, J., Mo, K.C., Ropelewski, C., Wang, J., Leetmaa, A., Reynolds, R., Jenne, R., Joseph, D., 1996. The NCEP/NCAR 40-year reanalysis project. Bull. Am. Meteorol. Soc. 77, 437–471.

Kerminen, V.M., Hillamo, R., Teinilä, K., Pakkanen, T., Allegrini, I., Sparapani, R., 2001. Ion balances of size-resolved tropospheric aerosol samples: implications for the acidity and atmospheric processing of aerosols. Atmos. Environ. 35 (31), 5255–5265.

Khan, M.B., Masiol, M., Formenton, G., Di Gilio, A., de Gennaro, G., Agostinelli, C., Pavoni, B., 2016. Carbonaceous PM2.5 and secondary organic aerosol across the Veneto region (NE Italy). Sci. Total Environ. 542, 172–181.

Kim, E., Hopke, P.K., Edgerton, E.S., 2003. Source identification of atlanta aerosol by positive matrix factorization. J. Air Waste Manag. Assoc. 53, 731–739.

Kleindienst, T.E., Smith, D.F., Li, W., Edney, E.O., Driscoll, D.J., Speer, R.E., Weathers, W.S., 1999. Secondary organic aerosol formation from the oxidation of aromatic hydrocarbons in the presence of dry submicron ammonium sulfate aerosol. Atmos. Environ. 33, 3669–3681.

Kroll, J.H., Seinfeld, J.H., 2008. Chemistry of secondary organic aerosol: formation and evolution of low-volatility organics in the atmosphere. Atmos. Environ. 42, 3593–3624.

Kukutschová, J., Filip, P.F., 2018. Review of Brake Wear Emissions: A Review of Brake Emission Measurement Studies: Identification of Gaps and Future Needs. In: Amato, F., (Ed.), Non-Exhaust Emissions (pp. 123-146), Academic Press.

Kuwata, M., Liu, Y., McKinney, K., Martin, S.T., 2015. Physical state and acidity of inorganic sulfate can regulate the production of secondary organic material from isoprene photooxidation products. Phys. Chem. Chem. Phys. 17, 5670–5678.

Lakey, P.S., Berkemeier, T., Tong, H., Arangio, A.M., Lucas, K., Pöschl, U., Shiraiwa, M., 2016. Chemical exposure-response relationship between air pollutants and reactive oxygen species in the human respiratory tract. Sci. Rep. 6, 32916.

Larsen, B.R., Gilardoni, S., Stenström, K., Niedzialek, J., Jimenez, J., Belis, C.A., 2012. Sources for PM air pollution in the Po Plain, Italy: II. Probabilistic uncertainty characterization and sensitivity analysis of secondary and primary sources. Atmos. Environ. 50, 203–213.

Li, W., Xu, L., Liu, X., Zhang, J., Lin, Y., Yao, X., Gao, H., Zhang, D., Chen, J., Wang, W., Harrison, R.M., 2017. Air pollution–aerosol interactions produce more bioavailable iron for ocean ecosystems. Sci. Adv. 3, (3) e1601749.

Maindonald, J.H., Braun, W.J., 2019. DAAG: Data Analysis and Graphics Data and Functions. R package version 1.22.1. Available at: https://CRAN.R-project.org/package=DAAG (last access on July 2019).

Mangiafico, S., 2019. rcompanion: Functions to Support Extension Education Program Evaluation. R package version 2.1.1. Available at: https://CRAN.R-project.org/package=rcompanion (last access on July 2019).

Masiol, M., Squizzato, S., Ceccato, D., Rampazzo, G., Pavoni, B., 2012. Determining the influence of different atmospheric circulation patterns on PM10 chemical composition in a source apportionment study. Atmos. Environ. 63, 117–124.

Masiol, M., Formenton, G., Pasqualetto, A., Pavoni, B., 2013. Seasonal trends and spatial variations of PM10-bounded polycyclic aromatic hydrocarbons in Veneto Region, Northeast Italy. Atmos. Environ. 79, 811–821.

Masiol, M., Squizzato, S., Rampazzo, G., Pavoni, B., 2014a. Source apportionment of PM2.5 at multiple sites in Venice (Italy): spatial variability and the role of weather. Atmos. Environ. 98, 78–88.

Masiol, M., Agostinelli, C., Formenton, G., Tarabotti, E. and Pavoni, B., 2014b. Thirteen years of air pollution hourly monitoring in a large city: Potential sources, trends, cycles and effects of car-free days. Sci. Total Environ., 494–495, 84–96.

Masiol, M., Benetello, F., Harrison, R.M., Formenton, G., De Gaspari, F., Pavoni, B., 2015. Spatial, seasonal trends and transboundary transport of PM2.5 inorganic ions in the Veneto region (Northeastern Italy). Atmos. Environ. 117, 19–31.

Masiol, M., Squizzato, S., Formenton, G., Harrison, R.M., Agostinelli, C., 2017. Air quality across a European hotspot: spatial gradients, seasonality, diurnal cycles and trends in the Veneto region, NE Italy. Sci. Total Environ. 576, 210–224.

Moldanová, J., Fridell, E., Popovicheva, O., Demirdjian, B., Tishkova, V., Faccinetto, A., Focsa, C., 2009. Characterisation of particulate matter and gaseous emissions from a large ship diesel engine. Atmos. Environ. 43 (16), 2632–2641.

Moreno, T., Alastuey, A., Querol, X., Font, O., Gibbons, W., 2007. The identification of metallic elements in airborne particulate matter derived from fossil fuels at Puertollano, Spain. Int. J. Coal Geol. 71 (2–3), 122–128.

Moreno, T., Querol, X., Alastuey, A., de la Rosa, J., de la Campa, A.M.S., Minguillón, M., Pandolfi, M., González-Castanedo, Y., Monfort, E., Gibbons, W., 2010. Variations in vanadium, nickel and lanthanoid element concentrations in urban air. Sci. Total Environ. 408 (20), 4569–4579.

Nenes, A., Pandis, S.N., Pilinis, C., 1998. ISORROPIA: a new thermodynamic equilibrium model for multiphase multicomponent inorganic aerosols. Aquat. Geochem. 4 (1), 123–152.

Nenes, A., Krom, M.D., Mihalopoulos, N., Cappellen, P.V., Shi, Z., Bougiatioti, A., Zarmpas, P., Herut, B., 2011. Atmospheric acidification of mineral aerosols: a source of bioavailable phosphorus for the oceans. Atmos. Chem. Phys. 11 (13), 6265–6272.

Oakes, M., Ingall, E.D., Lai, B., Shafer, M.M., Hays, M.D., Liu, Z.G., Russell, A.G., Weber, R.J., 2012. Iron solubility related to particle sulfur content in source emission and ambient fine particles. Environ. Sci. Technol. 46 (12), 6637–6644.

Paatero, P., 1997. Least squares formulation of robust non-negative factor analysis. Chemometrics and Intelligent Laboratory Systems 37, 23–35.

Paatero, P., Hopke, P.K., 2003. Discarding or downweighting high- noise variables in factor analytic models. Anal. Chim. Acta 490, 277–289.

Paatero, P., Tapper, U., 1994. Positive matrix factorization: A non-negative factor model with optimal utilization of error estimates of data values. Environmetrics 5, 111–126.

Paatero, P., Hopke, P.K., Begum, B.A., Biswas, S.W., 2005. A graphical diagnostic method for assessing the rotation in factor analytical models of atmospheric pollution. Atmos. Environ. 39, 193–201.

Paatero, P., Eberly, S., Brown, S.G., Norris, G.A., 2014. Methods for estimating uncertainty in factor analytic solutions. Atmos. Meas. Tech. 7, 781–797.

Padoan, E., Amato, F., 2018. Vehicle Non-Exhaust Emissions: Impact on Air Quality. In: Non-Exhaust Emissions (pp. 21-65), Amato F. (Ed.), Academic Press.

Panko, J., Kreider, M., Kenneth, U., 2018. Review of Tire Wear Emissions: A Review of Tire Emission Measurement Studies: Identification of Gaps and Future Needs. In: Non-Exhaust Emissions (pp. 147-170), Amato F. (Ed.), Academic Press.

Pant, P., Harrison, R.M., 2013. Estimation of the contribution of road traffic emissions to particulate matter concentrations from field measurements: a review. Atmos. Environ. 77, 78–97.

Pecorari, E., Squizzato, S., Masiol, M., Radice, P., Pavoni, B., Rampazzo, G., 2013. Using a photochemical model to assess the horizontal, vertical and time distribution of PM2.5 in a complex area: relationships between the regional and local sources and the meteorological conditions. Sci. Total Environ. 443, 681–691.

Pernigotti, D., Georgieva, E., Thunis, P., Bessagnet, B., 2012. Impact of meteorology on air quality modeling over the Po valley in northern Italy. Atmos. Environ. 51, 303–310.

Perrino, C., Catrambone, M., Dalla Torre, S., Rantica, E., Sargolini, T., Canepari, S., 2014. Seasonal variations in the chemical composition of particulate matter: a case study in the Po Valley. Part I: macro-components and mass closure. Environ. Sci. Pollut. Res. 21 (6), 3999–4009.

Perrone, M.G., Larsen, B.R., Ferrero, L., Sangiorgi, G., De Gennaro, G., Udisti, R., Zangrando, R., Gambaro, A., Bolzacchini, E., 2012. Sources of high PM2. 5 concentrations in Milan, Northern Italy: molecular marker data and CMB modelling. Sci. Total Environ. 414, 343–355.

Piazzalunga, A., Anzano, M., Collina, E., Lasagni, M., Lollobrigida, F., Pannocchia, A., Fermo, P., Pitea, D., 2013. Contribution of wood combustion to PAH and PCDD/F concentrations in two urban sites in Northern Italy. J. Aerosol Sci. 56, 30–40.

Pietr ogrande, M.C., Bacco, D., Ferrari, S., Kaipainen, J., Ricciardelli, I., Riekkola, M.L., Trentini, A., Visentin, M., 2015. Characterization of atmospheric aerosols in the Po Valley during the supersito campaigns—Part 3: Contribution of wood combustion to wintertime atmospheric aerosols in Emilia Romagna region (Northern Italy). Atmos. Environ. 122, 291–305.

Polissar, A.V., Hopke, P.K., Paatero, P., Malm, W.C., Sisler, J.F., 1998. Atmospheric aerosol over Alaska: 2. Elemental composition and sources. J. Geophys. Res.: Atmos. 103, 19045–19057.

R Core Team, 2018. R: A language and environment for statistical computing. R Foundation for Statistical Computing, Vienna, Austria. Available at: https://www.R-project.org/ (last access on July 2019).

Reff, A., Eberly, S.I., Bhave, P.V., 2007. Receptor modeling of ambient particulate matter data using positive matrix factorization: review of existing methods. J. Air Waste Manag. Assoc. 57, 146–154.

Rolph, G., Stein, A., Stunder, B., 2017. Real-time Environmental Applications and Display sYstem: READY. Environ. Modell. Software 95, 210–228.

Seibert, P., H., K.-K., Baltensperger, U., Jost, D.T., Schwikowski, M., Kasper, A. and Puxbaum, H., 1994. Trajectory analysis of aerosol measurements at high alpine sites. In: Transport and Transformation of Pollutants in the Troposphere, Borrel P.M., Borrell P., Cvitas T., Seiler W. (Eds.), pp. 689–693.

Seinfeld, J.H., Pandis, S.N., 2016. Atmospheric Chemistry and Physics: From Air Pollution to Climate Change. John Wiley & Sons.

Shi, Z., Krom, M.D., Jickells, T.D., Bonneville, S., Carslaw, K.S., Mihalopoulos, N., Baker, A.R., Benning, L.G., 2012. Impacts on iron solubility in the mineral dust by processes in the source region and the atmosphere: a review. Aeolian Res. 5, 21–42.

Shi, G., Xu, J., Peng, X., Xiao, Z., Chen, K., Tian, Y., Guan, X., Feng, Y., Yu, H., Nenes, A., Russell, A.G., 2017. pH of aerosols in a polluted atmosphere: source contributions to highly acidic aerosol. Environ. Sci. Technol. 51 (8), 4289–4296.

Shi, X., Nenes, A., Xiao, Z., Song, S., Yu, H., Shi, G., Zhao, Q., Chen, K., Feng, Y., Russell, A.G., 2019. High-resolution datasets unravel the effects of sources and meteorological conditions on nitrate and its gas-particle partitioning. Environ. Sci. Technol. 53, 3048–3057.

Squizzato, S., Masiol, M., 2015. Application of meteorology-based methods to determine local and external contributions to particulate matter pollution: a case study in Venice (Italy). Atmos. Environ. 119, 69–81.

Squizzato, S., Masiol, M., Brunelli, A., Pistollato, S., Tarabotti, E., Rampazzo, G., Pavoni, B., 2013. Factors determining the formation of secondary inorganic aerosol: a case study in the Po Valley (Italy). Atmos. Chem. Phys. 13 (4), 1927–1939.

Squizzato, S., Masiol, M., Visin, F., Canal, A., Rampazzo, G., Pavoni, B., 2014. The PM2.5 chemical composition in an industrial zone included in a large urban settlement: main sources and local background. Environ. Sci. Processes Impacts 16, 1913–1922.

Squizzato, S., Masiol, M., Agostini, C., Visin, F., Formenton, G., Harrison, R.M., Rampazzo, G., 2016. Factors, origin and sources affecting PM1 concentrations and composition at an urban background site. Atmos. Res. 180, 262–273.

Squizzato, S., Cazzaro, M., Innocente, E., Visin, F., Hopke, P.K., Rampazzo, G., 2017. Urban air quality in a mid-size city—PM2. 5 composition, sources and identification of impact areas: From local to long range contributions. Atmos. Res. 186, 51–62.

Stein, A.F., Draxler, R.R., Rolph, G.D., Stunder, B.J.B.B., Cohen, M.D., Ngan, F., 2015. NOAA's hysplit atmospheric transport and dispersion modeling system. Bull. Am. Meteorol. Soc. 96, 2059–2077.

Stelson, A.W., Seinfeld, J.H., 1982. Relative humidity and temperature dependence of the ammonium nitrate dissociation constant. Atmos. Environ. 16, 983–992.

Stohl, A., 1996. Trajectory statistics – a new method to establish source-receptor relationships of air pollutants and its application to the transport of particulate sulfate in Europe. Atmos. Environ. 30, 579–587.

Stortini, A.M., Freda, A., Cesari, D., Cairns, W.R.L., Contini, D., Barbante, C., Prodi, F., Cescon, P., Gambaro, A., 2009. An evaluation of the PM2.5 trace elemental composition in the Venice Lagoon area and an analysis of the possible sources. Atmos. Environ. 43 (40), 6296–6304.

Thorpe, A., Harrison, R.M., 2008. Sources and properties of non-exhaust particulate matter from road traffic: a review. Sci. Total Environ. 400, 270–282.

Tositti, L., Brattich, E., Masiol, M., Baldacci, D., Ceccato, D., Parmeggiani, S., Stracquadanio, M., Zappoli, S., 2014. Source apportionment of particulate matter in a large city of southeastern Po Valley (Bologna, Italy). Environ. Sci. Pollut. Res. 21 (2), 872–890.

Turnock, S.T., Butt, E.W., Richardson, T.B., Mann, G.W., Reddington, C.L., Forster, P.M., Haywood, J., Crippa, M., Janssens-Maenhout, G., Johnson, C.E., Bellouin, N., 2016. The impact of European legislative and technology measures to reduce air pollutants on air quality, human health and climate. Environ. Res. Lett. 11, (2) 024010.

Vecchi, R., Chiari, M., D'Alessandro, A., Fermo, P., Lucarelli, F., Mazzei, F., Nava, S., Piazzalunga, A., Prati, P., Silvani, F., Valli, G., 2008. A mass closure and PMF source apportionment study on the sub-micron sized aerosol fraction at urban sites in Italy. Atmos. Environ. 42 (9), 2240–2253.

Venables, W.N., Ripley, B.D., 2002. Modern Applied Statistics with S. Springer, New York.

Weber, R.J., Guo, H., Russell, A.G., Nenes, A., 2016. High aerosol acidity despite declining atmospheric sulfate concentrations over the past 15 years. Nat. Geosci. 9 (4), 282.

Wickham, H., 2007. Reshaping data with the reshape package. J. Stat. Softw. 21 (12), 1–20.

Wickham, H., 2011. The split-apply-combine strategy for data analysis. J. Stat. Softw. 40 (1), 1–29.

Wickham, H., 2018. scales: Scale Functions for Visualization. R package version 1.0.0. Available at: https://CRAN.R-project.org/package=scales (last access on July 2019).

WMO/IGAC, 2012. GAW Report No. 205 WMO/IGAC Impacts of Megacities on Air Pollution and Climate. GAW Rep. 41.

Yin, J., Harrison, R.M., 2008. Pragmatic mass closure study for PM1.0, PM2.5 and PM10 at roadside, urban background and rural sites. Atmos. Environ. 42, 980–988.

Zeileis, A., Grothendieck, G., 2005. zoo: S3 infrastructure for regular and irregular time series. J. Stat. Softw. 14 (6), 1–27.

Zhang, Q., Jimenez, J.L., Worsnop, D.R., Canagaratna, M., 2007. A case study of urban particle acidity and its influence on secondary organic aerosol. Environ. Sci. Technol. 41, 3213–3219.